



Optimizing the Relaxivity of MRI Probes at High Magnetic Field Strengths With Binuclear Gd^{III} Complexes

Loredana Leone¹, Giuseppe Ferrauto², Maurizio Cossi¹, Mauro Botta¹ and Lorenzo Tei^{1*}

¹ Dipartimento di Scienze e Innovazione Tecnologica, Università degli Studi del Piemonte Orientale "Amedeo Avogadro," Alessandria, Italy, ² Department of Molecular Biotechnology and Health Sciences, Molecular Imaging Centre, University of Torino, Torino, Italy

OPEN ACCESS

Edited by:

Carlos Lodeiro,
Faculdade de Ciências e Tecnologia
da Universidade Nova de Lisboa,
Portugal

Reviewed by:

Eurico J. Cabrita,
Faculdade de Ciências e Tecnologia
da Universidade Nova de Lisboa,
Portugal
Guo-Hong Tao,
Sichuan University, China

*Correspondence:

Lorenzo Tei
lorenzo.tei@uniupo.it

Specialty section:

This article was submitted to
Inorganic Chemistry,
a section of the journal
Frontiers in Chemistry

Received: 25 January 2018

Accepted: 19 April 2018

Published: 15 May 2018

Citation:

Leone L, Ferrauto G, Cossi M,
Botta M and Tei L (2018) Optimizing
the Relaxivity of MRI Probes at High
Magnetic Field Strengths With
Binuclear Gd^{III} Complexes.
Front. Chem. 6:158.
doi: 10.3389/fchem.2018.00158

The key criteria to optimize the relaxivity of a Gd(III) contrast agent at high fields (defined as the region ≥ 1.5 T) can be summarized as follows: (i) the occurrence of a rotational correlation time τ_R in the range of ca. 0.2–0.5 ns; (ii) the rate of water exchange is not critical, but a $\tau_M < 100$ ns is preferred; (iii) a relevant contribution from water molecules in the second sphere of hydration. In addition, the use of macrocycle-based systems ensures the formation of thermodynamically and kinetically stable Gd(III) complexes. Binuclear Gd(III) complexes could potentially meet these requirements. Their efficiency depends primarily on the degree of flexibility of the linker connecting the two monomeric units, the absence of local motions and the presence of contribution from the second sphere water molecules. With the aim to maximize relaxivity (per Gd) over a wide range of magnetic field strengths, two binuclear Gd(III) chelates derived from the well-known macrocyclic systems DOTA-monopropionamide and HPDO3A (Gd₂L1 and Gd₂L2, respectively) were synthesized through a multistep synthesis. Chemical Exchange Saturation Transfer (CEST) experiments carried out on Eu₂L2 at different pH showed the occurrence of a CEST effect at acidic pH that disappears at neutral pH, associated with the deprotonation of the hydroxyl groups. Then, a complete ¹H and ¹⁷O NMR relaxometric study was carried out in order to evaluate the parameters that govern the relaxivity associated with these complexes. The relaxivities of Gd₂L1 and Gd₂L2 (20 MHz, 298 K) are 8.7 and 9.5 mM⁻¹ s⁻¹, respectively, +77% and +106% higher than the relaxivity values of the corresponding mononuclear GdDOTAMAP-En and GdHPDO3A complexes. A significant contribution of second sphere water molecules was accounted for the strong relaxivity enhancement of Gd₂L2. MR phantom images of the dinuclear complexes compared to GdHPDO3A, recorded at 7 T, confirmed the superiority of Gd₂L2. Finally, ab initio (DFT) calculations were performed to obtain information about the solution structure of the dinuclear complexes.

Keywords: gadolinium, macrocyclic ligands, multimeric contrast agents, magnetic resonance imaging-high field, chemical exchange saturation transfer, relaxometry, DFT

INTRODUCTION

The success of Magnetic Resonance Imaging (MRI) as a clinical diagnostic technique is mainly related to its superb temporal and spatial resolution that allow the clear delineation and differentiation of soft tissues and to its low invasiveness that leads to high patient acceptability. MRI contrast agents (CAs) are used for a large fraction of clinical scans (40–50%) to increase tissue contrast on relaxation weighted images by shortening the relaxation times of the water molecules in their proximity. Some 400 million doses of gadolinium have been administered for MRI scans since 1988. Currently, clinically employed CAs are low molecular weight, nonspecific Gd^{III} complexes with polyaminocarboxylate ligands that are capable to enhance the longitudinal relaxation rate ($R_1 = 1/T_1$) of water protons in the extracellular space. The increase in R_1 induced by one millimolar concentration of the paramagnetic ion is called relaxivity (r_1), a key parameter that depends on several structural and dynamic features of the Gd^{III} complex. Among the most important are the molecular rotation (τ_R), the electronic relaxation times ($T_{1,2e}$) and the residence lifetime of the coordinated water molecule(s) (τ_M) (Caravan et al., 1999; Botta and Tei, 2012; Merbach et al., 2013).

Typically, the commercially available Gd-based CAs have limited contrast enhancement capability (r_1 about 3–4 mM⁻¹s⁻¹ at 0.47 T and 37°C), much lower than that theoretically attainable (Geraldès and Laurent, 2009). Furthermore, their relaxivity values steadily decrease with increasing the magnetic field strength, e.g., r_1 of GdHPDO3A at 11.7 T and 37°C is 2.9 mM⁻¹s⁻¹ (Delli Castelli et al., 2013). Therefore, over the years, great research efforts have been made to optimize the structural and dynamic properties of the Gd^{III} complexes in order to achieve higher relaxivities, in particular in the high fields range. However, the interplay of the different contributions often resulted in non-optimized systems or probes that afford remarkable results only for a specific application. For example, blood pool contrast agents, such as MS-325, were designed to exploit their strong binding to slow tumbling molecules (i.e., Human Serum Albumin) for MR angiographic applications (Caravan et al., 2002), but this strategy gives high longitudinal relaxivity between 0.5 and 1.0 T and then sharply drops with increasing field thus, at fields > 1.5 T, macromolecular agents are hardly superior to small molecular weight chelates.

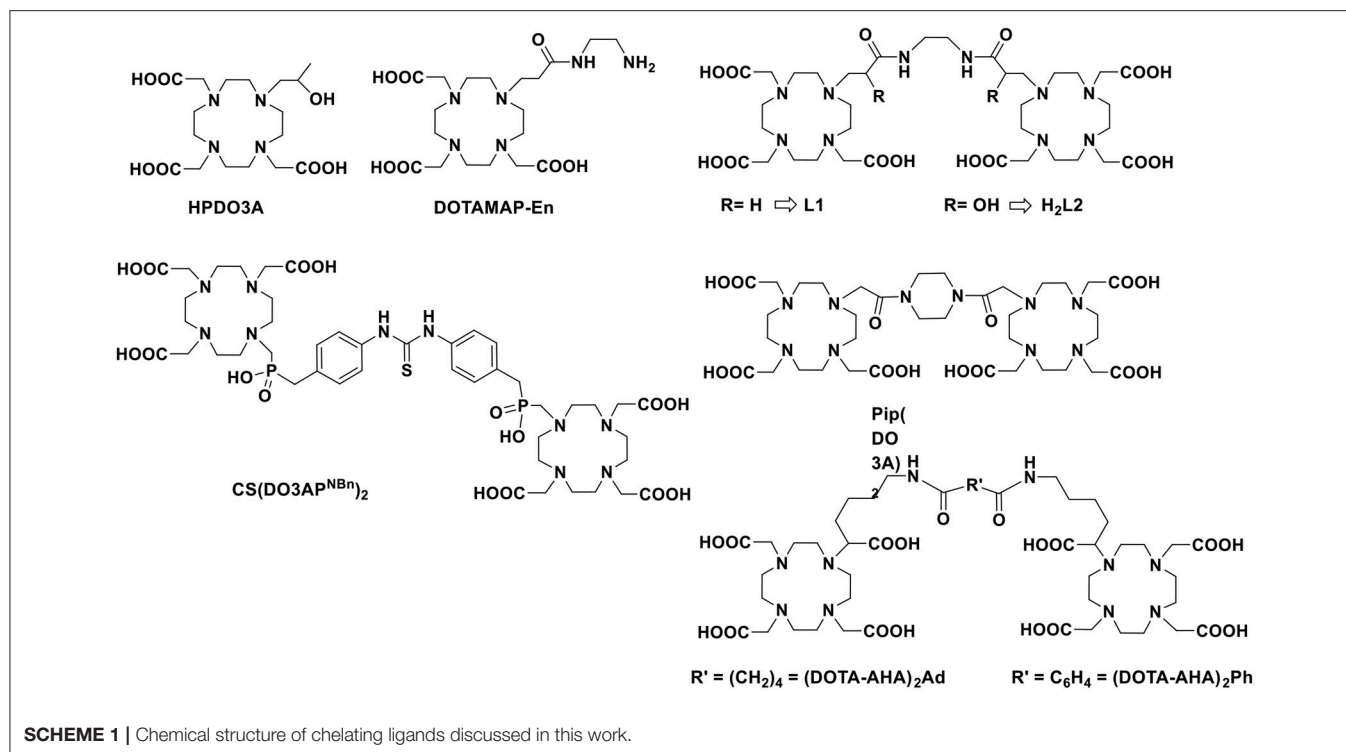
Nonetheless, although nowadays the majority of MRI scanners used in clinics operates at 1.5 T, more than one-quarter are 3 T machines and 7 T whole body human scanners are also available on the market. Therefore, a specific strategy for r_1 enhancement of metal-based probes at high field, i.e., a Gd-complex that will maintain its r_1 constant at least in the 1.5–3.0 T range, is extremely necessary to obtain a better contrast enhancement with lower amounts of CAs administered.

In recent reviews, it has been nicely shown that the use of systems with rotational correlation times in the range of ~0.5–2.0 ns and coordinated water molecule(s) in a relatively fast exchange rate ($\tau_M \sim 10$ –100 ns) would allow the increase of r_1 at magnetic field strengths > 1.5 T (Caravan et al., 2009; Helm, 2010). However, in accordance with recent investigations, we

surmised that ditopic Gd^{III} chelates with a molecular rotational correlation time (τ_R) in the range 0.2–0.5 ns (i.e., Gd-complexes with molecular mass in the range of ca. 1–3 kDa) and a short, rigid and hydrophilic linker between the two chelating units could represent an optimal solution. In fact, in such systems the rigidity of the spacer should reduce the local mobility of the monomeric Gd-units and enable a better correlation between global and local motions. Moreover, a hydrophilic spacer might favor the presence of a network of hydrogen bonded water molecules that can contribute greatly to the relaxivity through the second sphere contribution (Botta, 2000). A residence lifetime of the inner sphere water molecule (τ_M) preferably below 100 ns would complete the characteristics of these ditopic Gd^{III} chelates.

There are several approaches to design ditopic Gd-complexes as clearly delineated by Caravan and co-workers (Boros et al., 2012), being the one with an organic scaffold at the barycentre the most used strategy. In their example, they used an amino acid-like, fast exchanging Gd-complex (DOTAla) suitable for solid phase peptide synthesis and integration into hydrophilic polypeptide structures. They also investigated the possibility to rigidify the multimeric structure by forming disulphide bridges between cysteine moieties. Other examples of ditopic systems were reported by using GdDOTA-monoamide (Powell et al., 1996; Tei et al., 2009b), GdHPDO3A (Ranganathan et al., 1998), GdDOTA (Fontes et al., 2015) or GdDOTA-monophosphinate (Rudovský et al., 2006) derivatives linked by aliphatic or heterocyclic groups (**Scheme 1**). The relaxivity enhancement of these systems as compared to monomeric Gd-complexes was often very much dependent on the water exchange rate or on the rigidity of the linker. We were also inspired by the recently reported self-assembling of two oppositely charged macrocyclic Gd-chelates that resulted in a small-sized dimeric system with high relaxivity at high frequencies thanks to improved inner- and second-sphere relaxivity contributions (Lawson et al., 2015). Remarkably, the additional contribution of about 30–40% from water molecules in the second coordination sphere was considered responsible of the increased performance of the ditopic probe.

Finally, we must consider that the kinetic inertness toward dissociation/transmetallation reactions is a fundamental parameter to consider in the design of novel MRI probe to aim for *in vivo* applications. Therefore, although a couple of examples of kinetically inert $q = 2$ Gd-complexes have been reported (Tircsó et al., 2006; Vagner et al., 2016), we will concentrate on two well-established $q = 1$ systems based on the macrocyclic systems HPDO3A (10-(2-hydroxypropyl)-1,4,7-tetraazacyclododecane-1,4,7-triacetic acid) and DOTAMAP (1,4,7,10-tetraazacyclododecane-1-propionamido-4,7,10-triacetic acid). These two chelates have been chosen because GdHPDO3A is the well-established, clinically approved MRI agent ProHance commercialized by Bracco (Delli Castelli et al., 2013) and GdDOTAMAP has been reported as a kinetically inert and fast exchanging Gd-complex (Tei et al., 2009a, 2015) that has also been recently exploited for the synthesis of high relaxivity multimeric systems (Boros et al., 2012). Thus, we present here the synthesis of two new ditopic chelators **L1** (DOTAMAP)₂ and **H₂L2** (HPA-DO3A)₂ (**Scheme 1**) and a complete ¹H and ¹⁷O NMR relaxometric study on the Gd^{III} complexes and a



CEST characterization on Eu₂L₂. Furthermore, ab initio DFT calculations were used to obtain information on the structure of Gd₂L₂ in solution, on the possible presence of second hydration sphere water molecules and on the internal mobility of the chelates about the linker.

MATERIALS AND METHODS

All chemicals were purchased from Sigma-Aldrich or Alfa Aesar unless otherwise stated and were used without further purification. The ¹H and ¹³C NMR spectra were recorded using a Bruker Avance III 500 MHz (11.4 T) spectrometer equipped with 5mm PABBO probes and BVT-3000 temperature control unit. Chemical shifts are reported relative to TMS and were referenced using the residual proton solvent resonances. HPLC analyses and mass spectra were performed on a Waters HPLC-MS system equipped with a Waters 1525 binary pumps. Analytical measurements were carried out on a Waters Atlantis RPC18 column (5 μm 4.6 × 100 mm) and on a Waters Atlantis prep T3 OBD (5 μm 19 × 100 mm) for preparative purposes. Electrospray ionization mass spectra (ESI MS) were recorded using a SQD 3100 Mass Detector (Waters), operating in positive or negative ion mode, with 1% v/v formic acid in methanol as the carrier solvent.

1,2-Diacrylamidoethane

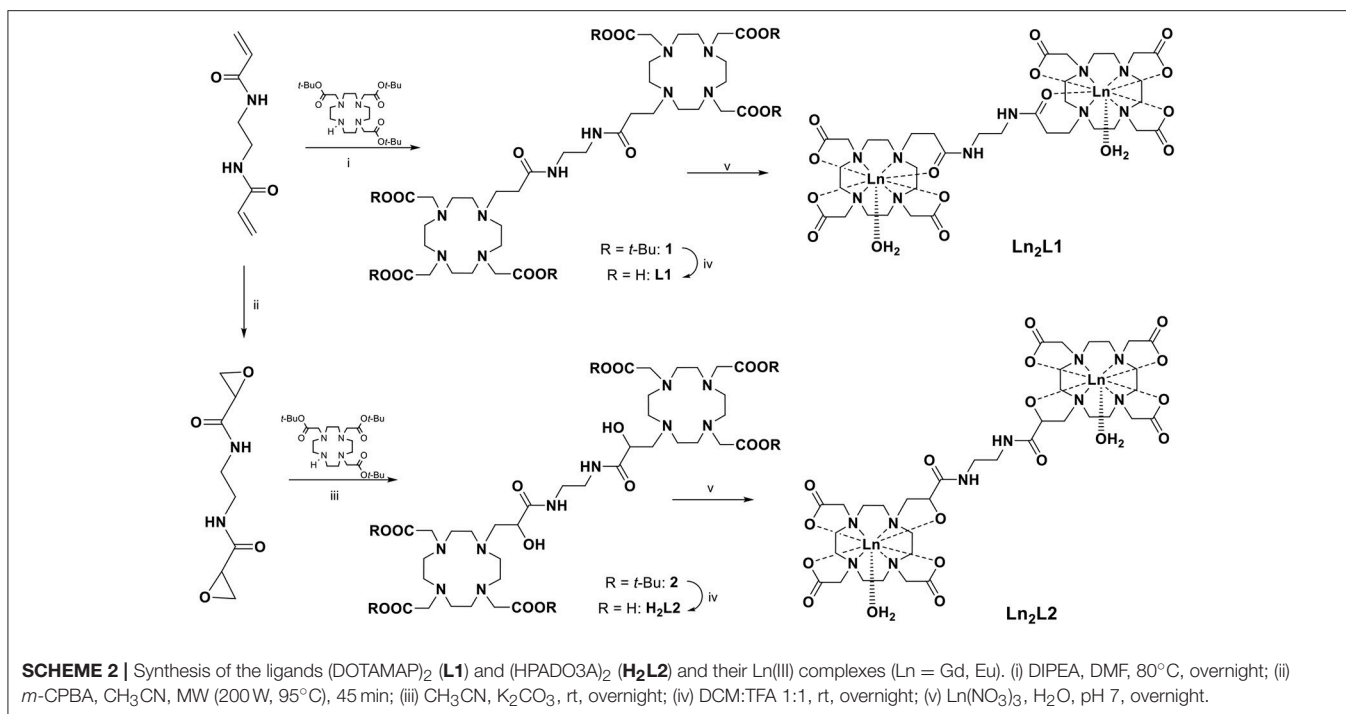
To a stirred solution of ethylenediamine (0.110 mL, 100 mg, 1.66 mmol) and K₂CO₃ (0.7 g, 5 mmol) in dry CH₃CN (2 mL), acryloyl chloride (0.3 mL, 0.33 g, 3.65 mmol) was added dropwise at 0°C and left stirring at r.t overnight, then filtered and

evaporated in vacuo to obtain the pure product. Analytical HPLC: Pump A: NH₄OAc (7 mM, pH 5.5); Pump B = ACN; flow = 1 mL/min; 0–10 min = 100% A; 10–15 min = 100% B; 15–24 min = 100% B; 24–25 min = 100% A; t_r = 17.18 min.

Yield 250 mg (90%); MS (ESI⁺): *m/z*: 169.17 [M+H]⁺ ¹H NMR (500MHz, CD₃CN, 25°C): δ = 6.85 (brs, 1H; NH-), 6.14 (m, ²J (H,H) = 2.5 Hz, ³J (H,H) = 4.8 Hz, 2H; CH₂ = CH), 5.59 (dd, ²J (H,H) = 2.5 Hz, ³J (H,H) = 4.8 Hz, 1H; CH₂ = CH-), 3.33 (d, ³J (H,H) = 2.8 Hz; 2H, CO-NH-CH₂) ppm. ¹³C{¹H}NMR (125MHz, CD₃CN, 25°C): δ = 166.6 (CO-NH-CH₂), 132.4 (CH₂ = CH), 125.9 (CH₂ = CH), 39.9 (-CO-NH-CH₂-) ppm.

Gd₂(DOTAMAP)₂ (Gd₂L1)

A solution of DO3A(t-Bu)₃ (50 mg, 0.097 mmol) and DIPEA (30 μL, 0.17 mmol) in DMF (2.5 mL) was added dropwise to 1,2-diacrylamidoethane (7 mg, 0.044 mmol) in DMF (1 mL) under N₂. The reaction was allowed to stir at 80°C overnight. Then, the crude mixture was evaporated in vacuo and the resulting oil was dissolved in a solution 1:1 of DCM: TFA and stirred at room temperature overnight. Then, the solvent mixture was evaporated under reduced pressure to obtain a yellow oil that was dissolved in H₂O. Complexation was performed directly on the unpurified sample: Ln(NO₃)₃ (Ln = Gd and Eu; 0.5 M aqueous solutions) was added to a solution of the ligand in water (2 mL). The pH was gradually adjusted to 7 and the solution stirred at room temperature overnight. The pH was then increased to 10 to precipitate excess Ln^{III} as hydroxide. The solution was centrifuged (4,000 rpm, 3 min, r.t.) and the supernatant filtered through a 0.2 μm filter. The pH was re-adjusted to 7 and the solvent removed in vacuo. The Ln^{III}-complexes were purified on



preparative HPLC with the following method: Pump A: NH₄OAc (7 mM, pH 5.5); Pump B = ACN; flow = 20 mL/min; 0–4 min = 100% A; 4–14 min = 100% B; 14–15 min = 100% B; 15–16 min = 100% A. Gd₂L1: t_r = 6.69 min; Yield: 30% (16 mg, 0.014 mmol). MS (ESI⁺): m/z : 585.2 [(M+2H)/2]⁺. Eu₂L1: t_r = 7.01 min Yield: 25% (12 mg, 0.010 mmol). MS (ESI⁺): m/z : 580.1 [(M+2H)/2]⁺.

***N,N'*-(ethane-1,2-diyl)bis(oxirane-2-carboxamide)**

1,2-diacrylamidoethane (100 mg, 0.6 mmol) and *m*-chloroperbenzoic acid (1 g, 4.76 mmol) were dissolved in CH₃CN (3 mL) and reacted in a MW (CEM, DISCOVER SP) reactor (45 min, 95°C, 200 W). The solution was then evaporated in vacuo, dissolved in 1 mL H₂O:ACN (1:1) and purified in preparative HPLC with the following method: Pump A: NH₄OAc (7 mM, pH 5.5); Pump B = ACN; flow = 20 mL/min; 0–10 min = 100% A; 10–15 min = 100% B; 15–24 min = 100% B; 24–25 min = 100% A; t_r = 13.06 min. Forty-eight milligram (0.24 mmol, 40% yield) of a white powder were obtained. MS (ESI⁺): m/z : 201.25 [M+H]⁺; ¹H NMR (500 MHz, CD₃CN, 25°C): δ = 3.27 (m, 2H; CO-NH-CH₂), 3.20 (m, 1H; CO-CH-CH₂), 2.89, 2.73 (m,m, 2H; CO-CH-CH₂) ppm. ¹³C{¹H}NMR (125 MHz, CD₃CN, 25°C): δ = 170.6 (CO-NH-CH₂), 49.9 (CO-CH-CH₂) 47.6 (CO-CH-CH₂), 39.6 (CO-NH-CH₂) ppm.

(HPA-DO3A)₂(*t*Bu)₆

N,N'-(ethane-1,2-diyl)bis(oxirane-2-carboxamide) (18 mg, 0.09 mmol) was dissolved in dry CH₃CN (5 mL) and K₂CO₃ (50 mg, 0.36 mmol) and DO3A(*t*-Bu)₃ (92 mg, 0.18 mmol) were added to the solution and stirred overnight at room temperature. After

filtration and evaporation under reduced pressure, the mixture was purified on silica (CH₃CN: NH₃ (10%)) to give the product **2**. Analytical HPLC: Pump A: H₂O (0.1% TFA); Pump B = MeOH; flow = 1 mL/min; 0–3 min = 70% A; 3–18 min = 100% B; 18–24 min = 100% B; 24–25 min = 70% A; t_r = 14.58 min. 28 mg (0.023 mmol, 25% yield) of a pale yellow oil were obtained. MS (ESI⁺): m/z : 615.8 [(M+2H)/2]⁺. ¹H NMR (500 MHz, CD₃CN, 25°C): δ = 3.89 (dd, 2H; N-CH₂-CH-CO-), 3.29 (m, 4H; N-CH₂-CH-CO), 3.20 (m, 12H; N-CH₂-CO-OC(CH₃)₃), 2.68–2.84 (m, 32H; cyclen), 1.44 (s, 54H; N-CH₂-CO-OC(CH₃)₃) ppm. ¹³C{¹H}NMR (125 MHz, CD₃CN, 25°C): δ = 174.8 (N-CH₂-CO-OC(CH₃)₃), 172.0 (N-CH₂-CH-CO); 81.1 (N-CH₂-CO-OC(CH₃)₃), 71.0 (-N-CH₂-CH-CO), 58.7 (N-CH₂-CH-CO), 58.1 (N-CH₂-CO-OC(CH₃)₃), 53.8, 52.9, 52.8.

(HPA-DO3A)₂ (H₂L2)

Compound **2** (28 mg, 0.023 mmol) was dissolved in a 1:1 solution of DCM:TFA and stirred overnight at room temperature. After evaporation under reduced pressure, ligand **H₂L2** was obtained in 95% yield (18 mg, 0.021 mmol). MS (ESI⁺): m/z : 447.8 [(M+2H)/2]⁺; ¹H NMR (500 MHz, CD₃CN, 25°C): δ = 4.62 (dd, 2H; N-CH₂-CH-CO), 4.12 (m, 4H; N-CH₂-CH-CO), 3.61 (m, 12H; N-CH₂-COOH, 12H), 3.15–3.50 (m, 32H; cyclen), ppm. ¹³C{¹H}NMR (125 MHz, CD₃CN, 25°C): δ = 173.2 (N-CH₂-CH-CO), 173.2 (N-CH₂-CO-OH), 66.4 (N-CH₂-CH-CO), 55.4 (N-CH₂-CH-CO-), 54.4 (N-CH₂-COOH), 53.2, 51.0, 50.3, 48.7, (cyclen), 38.6 (CO-NH-CH₂) ppm.

Ln(III) Complexes

Ln(NO₃)₃ (Ln = Gd and Eu; 0.5 M aqueous solutions) was added to a solution of the ligand in water (2 mL). The pH was gradually adjusted to 7 and the solution stirred at room temperature

overnight. The pH was then increased to 10 to precipitate excess Ln^{III} as hydroxide. The solution was centrifuged (4,000 rpm, 3 min, r.t.) and the supernatant filtered through a $0.2\ \mu\text{m}$ filter. The pH was re-adjusted to 7 and the solvent removed in vacuo. Analytical HPLC: Pump A: H_2O ; Pump B = MeOH; flow = 1 mL/min; 0–3 min = 100% A; 3–18 min = 100% B. $\text{Gd}_2\text{L2}$: $t_r = 9.35$ min. MS (ESI⁺): m/z : 600.98 [(M+2H)/2]⁺; $\text{Eu}_2\text{L2}$: $t_r = 9.01$ min. MS (ESI⁺): m/z : 596.68 [(M+2H)/2]⁺. The concentration of Ln-complexes was assessed by using the Evan's method.

Chemical Exchange Saturation Transfer (CEST) Experiment

Z-spectra of $\text{Eu}_2\text{L2}$ water solutions at different pH in a range between 4.0 and 9.1 were acquired at 21°C, 7T on a Bruker Avance 300 spectrometer equipped with a microimaging probe. A frequency offset range of ± 100 ppm was investigated. A typical RARE (Rapid Acquisition with Refocused Echoes) spin-echo sequence with TE 3 ms, TR 5 s and RARE factor 16 was used. An isotropic 64×64 acquisition matrix with a FOV of 12 mm and a slice thickness of 1 mm was used. The whole sequence was preceded by a saturation scheme consisting of a continuous rectangular wave pulse 2 s long with a radiofrequency B_1 field of $12\ \mu\text{T}$. The Z-spectra were interpolated by smoothing splines to identify the zero-offset on a pixel-by-pixel basis of the bulk water and, then, to assess the correct ST% value over the entire range of frequency offsets investigated. Custom-made software, compiled in the Matlab platform (Mathworks Inc., Natick, MA), was used (Stancanello et al., 2008; Terreno et al., 2009). The extent of CEST effect was calculated as follows:

$$\text{ST}\% = \left(1 - \frac{M_s}{M_0}\right) \times 100 \quad (1)$$

where M_s is the intensity of the bulk water NMR signal after the irradiation on resonance ($\Delta\omega$) of the mobile proton pool and M_0 is the intensity of the bulk water NMR signal after the irradiation at the opposite frequency ($-\Delta\omega$).

Relaxometric Measurements

The water proton longitudinal relaxation rates as a function of the magnetic field strength were measured in non-deuterated aqueous solutions on a Fast Field-Cycling Stelar SmarTracer relaxometer (Stelar s.r.l., Mede (PV), Italy) over a continuum of magnetic field strengths from 0.00024 to 0.25 T (corresponding to 0.01–10 MHz proton Larmor frequencies). The relaxometer operates under computer control with an absolute uncertainty in $1/T_1$ of $\pm 1\%$. Additional longitudinal relaxation data in the range 20–70 MHz were obtained on a Stelar Relaxometer connected to a Bruker WP80 NMR electromagnet adapted to variable-field measurements. The exact concentration of Gd(III) was determined by measurement of bulk magnetic susceptibility shifts of a *t*BuOH signal or by inductively coupled plasma mass spectrometry (ICP-MS, Element-2, Thermo-Finnigan, Rodano (MI), Italy). Sample digestion was performed with concentrated HNO_3 (70%, 2 mL) under microwave heating at 160°C for 20 min (Milestone MicroSYNTH Microwave lab station equipped with

an optical fiber temperature control and HPR-1000/6M six position high pressure reactor, Bergamo, Italy). The ^1H T_1 relaxation times were acquired by the standard inversion recovery method with typical 90° pulse width of $3.5\ \mu\text{s}$, 16 experiments of 4 scans. The temperature was controlled with a Stelar VTC-91 airflow heater equipped with a calibrated copper-constantan thermocouple (uncertainty of $\pm 0.1^\circ\text{C}$).

Variable-temperature ^{17}O NMR measurements were recorded on a Bruker Avance III spectrometer (11.7T) equipped with a 5 mm probe and standard temperature control unit. Aqueous solutions of the complexes containing 2.0% of the ^{17}O isotope (Cambridge Isotope) were used. The observed transverse relaxation rates were calculated from the signal width at half-height.

MR-Phantom Imaging

MR images of capillaries filled with 1.5 mM water solutions of $\text{Gd}_2\text{L1}$, $\text{Gd}_2\text{L2}$, or ProHance were acquired at 21°C, 7T on a Bruker Avance 300 spectrometer equipped with a microimaging probe. T_{2W} images were acquired by using a standard RARE (Rapid Acquisition with Refocused Echoes) sequence with the following parameters: TR = 5,000 ms, TE = 5.5 ms, FOV = 1×1 cm, slice thickness = 1 mm, RARE factor = 32, matrix size 128×128 . T_{1W} images were acquired by using a standard MSME (multi-slice multi-echo) sequence with the following parameters: TR = 50 ms, TE = 3.3 ms, FOV = 1×1 cm, slice thickness = 1 mm, matrix size 128×128 . T_1 values were measured by using a Saturation Recovery Spin Echo sequence with the following parameters: TE = 3.8 ms, 16 variable TR ranging from 50 to 5,000 ms, FOV = 1×1 cm, slice thickness = 1 mm).

Theoretical Modeling

Theoretical calculations were performed with Gaussian16 program (Frisch et al., 2016) at the density functional theory (DFT) level with the hybrid functional B3LYP (Becke, 1993), comprising a part of the exact exchange along with Becke's exchange and Lee-Yang-Parr correlation functionals. To limit the computational burden, the following effective core potentials were used for all the heavy atoms, along with the corresponding valence basis sets: LANL2DZ (Hay and Wadt, 1985a,b; Wadt and Hay, 1985) for C, N, O and MWB53 (Dolg et al., 1989) for Gd; long range solvent effects were computed for some systems through the polarizable continuum model (PCM) (Cossi et al., 2003); dispersion energies were included in all the calculations with the atom-atom semiempirical method and parameters proposed by Grimme (Grimme et al., 2010). When computing the complexation energies, Boys' counterpoise correction was applied to compensate the basis set superposition error (BSSE).

RESULTS AND DISCUSSION

Ligand Design and Synthesis

The ligand **L1** simply consists of two DOTA-monopropionamide units linked by an ethylene chain, therefore we expect that the relaxometric properties of the Gd complex would be consistent with a system with doubled molecular weight and similar

electronic and water exchange parameters with respect to the monomeric GdDOTAMAP complex (Tei et al., 2009a). On the other hand, in case of the ligand **H₂L₂**, there is a substantial change with respect to HPDO3A: a hydroxypropylamide group replaced the hydroxypropyl group in order to generate electron withdrawing effect on the coordinated hydroxyl group and therefore stronger coordinating ability. Moreover, the hydrophilic nature of the amide group is expected to contribute to the overall relaxivity of the system through formation of hydrogen bonds to second sphere water molecules. The two monomeric hydroxypropylamideDO3A chelators were linked again by a short ethylene moiety.

Both chelates were obtained from a bis-acrylamide, ethylene-bis-acrylamide, through a multistep synthesis (**Scheme 2**). The synthesis of (DOTAMAP)₂ (**L1**) started from the Michael addition of the bis-acrylamide to two equivalents of DO3A(*t*Bu)₃ in dimethylformamide (DMF) in the presence of diisopropylethylamine (DIPEA) to give the protected ditopic ligand (**1**), which was immediately subjected to deprotection by reaction with a 1:1 mixture of trifluoroacetic acid (TFA) and dichloromethane (DCM). Then, complexation with Gd(NO₃)₃ was carried out in water at pH 7 and at room temperature. The purification by semi-preparative HPLC-MS was carried out on the final complex to obtain Gd₂**L1** in 22% overall yield. The protected and deprotected ditopic intermediates were not isolated due to the tendency to elimination of the pendant arm to form again the acrylamide. This tendency is highly reduced in the presence of the Gd-complex, although solutions of Gd₂**L1** left in water at pH 7 for more than one month revealed the presence of a small amount of elimination products. A similar approach was followed by Meade and co-workers (Rotz et al., 2015) for the synthesis of a *N*-propargylpropionamide derivative used for the preparation of Gd-labeled gold nanoparticles.

On the other hand, to obtain (HPA-DO3A)₂ (**H₂L₂**), the bis-acrylamide was subjected to bis-epoxidation with meta-chloroperbenzoic acid (*m*-CPBA) in acetonitrile (ACN), using microwave heating (70 W, 90°C). After HPLC-MS purification the bis-epoxide was reacted with DO3A(*t*Bu)₃ in ACN in the presence of K₂CO₃ to give the protected HPA-DO3A dimer (**2**) which was purified by column chromatography and finally deprotected with a 1:1 mixture of TFA and DCM. Intermediates and final ligand were characterized by ESI mass spectrometry and ¹H and ¹³C NMR spectroscopy (Figures S7–S14). The Gd^{III} complex Gd₂**L2** was prepared at room temperature by adding Gd(NO₃)₃ to a solution of **H₂L₂** while maintaining the pH at 6.5 with diluted NaOH. The excess of free metal ions in the solution was precipitated by the addition of NaOH up to pH 9 and the Gd-complex was isolated through a successive centrifugation, filtration, and lyophilization.

Chemical Exchange Saturation Transfer (CEST) Measurements on Eu₂L₂

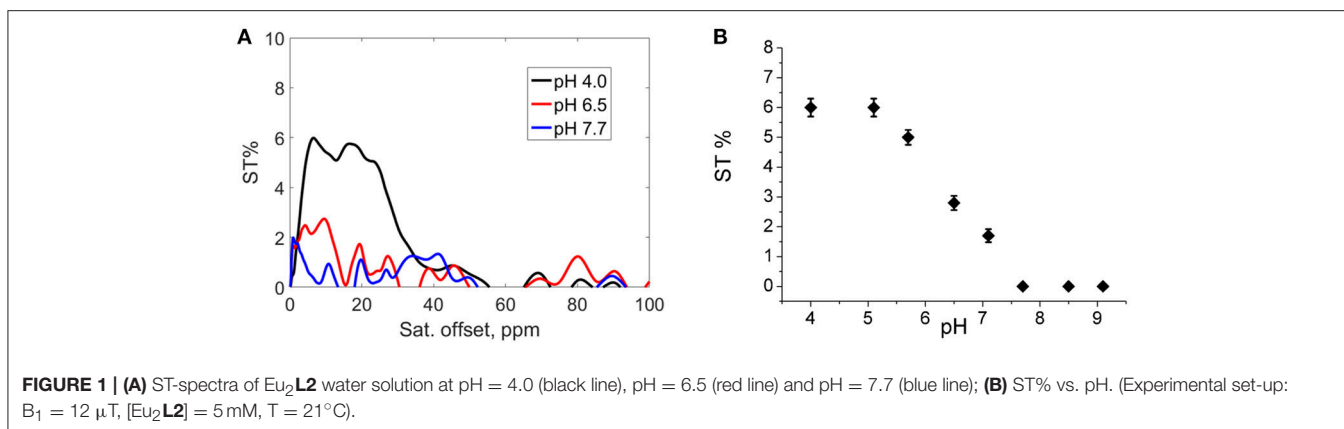
Lanthanide complexes of HPDO3A have been largely used as ParaCEST agents for cell labeling or extracellular/extravascular pH assessment in tumor models because the hydroxyl proton are close enough to the paramagnetic center to be able to generate CEST contrast (Nicholls et al., 2015; Pumphrey et al., 2016; Ferrauto et al., 2017). Moreover, as the exchange rate of the OH

proton is pH dependent, these chelates have been exploited as pH sensitive ParaCEST agents (Delli Castelli et al., 2014). Since the pK_a of these hydroxyl protons can be modulated by inserting electron withdrawing or donating groups in close proximity, the CEST contrast may be used to determine the deprotonation of the hydroxyl group. In the binuclear Ln₂**L2** complexes, the presence of an electron withdrawing amide group close to the hydroxyl group makes the OH proton very acid. Hence, it is reasonable to argue that this group is deprotonated at physiological pH values.

In order to obtain indirect insights into the exchangeable protons of the hydroxyl moieties, Z- and ST-spectra of Eu₂**L2** water solutions at different pH in a range between 4.0 and 9.1 were acquired. In CEST experiment, the resonance of exchangeable protons can be specifically saturated by a proper *rf* pulse. Saturated spins are transferred to bulk water through chemical exchange. In such a way, an indirect saturation of bulk water signal occurs, that can be observed in a ¹H-MR image. Z-spectra reports about bulk water signal as a function of the *rf* offset (Supplementary information, Figure S1). From Z-spectra, the symmetrical analysis allows obtaining ST-spectra, in which saturation transfer is plotted against the *rf* offset. Representative ST-spectra of Eu₂**L2** water solution at pH 4.0, 6.5 and 7.7 are reported in **Figure 1A**. The CEST effect is clearly visible at acid pH, barely visible at pH = 6.5 and completely absent at pH > 7.5. The ST% effect vs. pH is reported in **Figure 1B** showing the disappearance of CEST effect at neutral pH. Thus, this result is in line with the hypothesis of hydroxyl deprotonation at these pH values.

Relaxometric Measurements

The published value of *r*₁ for GdDOTAMAP-En (Tei et al., 2009a) and GdHPDO3A (Delli Castelli et al., 2013), at 0.47 T and 298 K, are 4.9 and 4.6 mM⁻¹ s⁻¹, respectively. These are typical values of the clinical MRI contrast agents, i.e., monohydrated low-molecular weight Gd^{III} chelates that tumble rapidly in solution and whose effectiveness as relaxation agents at high fields (≥ 0.47 T) is defined primarily by their rotational dynamics and thus by their molecular mass. In fact, the different *r*₁ values are associated with different values of τ_R, namely 79 and 65 ps for GdDOTAMAP-En and GdHPDO3A, respectively. The ionic (per Gd) *r*₁ values for the corresponding dimeric complexes, measured under identical experimental conditions, are 8.7 and 9.5 mM⁻¹ s⁻¹ for Gd₂**L1** and Gd₂**L2**, respectively. These values remain almost constant in the pH range 2–10 (Figure S2). These values correspond to relaxivity increases of +77% and +106% relative to the *r*₁ values of the corresponding mononuclear GdDOTAMAP-En and GdHPDO3A complexes. The relaxivity gain can be easily attributed to a longer value of the rotational correlation time associated with the increased molecular size, combined with the preservation of the same hydration state (*q* = 1) for each metal ion (Aime et al., 1992). From this information, we deduce that the binuclear complexes are remarkably rigid and compact, with a low degree of rotational flexibility about the linker. However, considering that only the inner-sphere contribution to relaxivity depends on τ_R, while the outer-sphere contribution remains almost unchanged, the



particularly strong r_1 enhancement measured for $\text{Gd}_2\text{L2}$ might suggest the presence of an additional contribution.

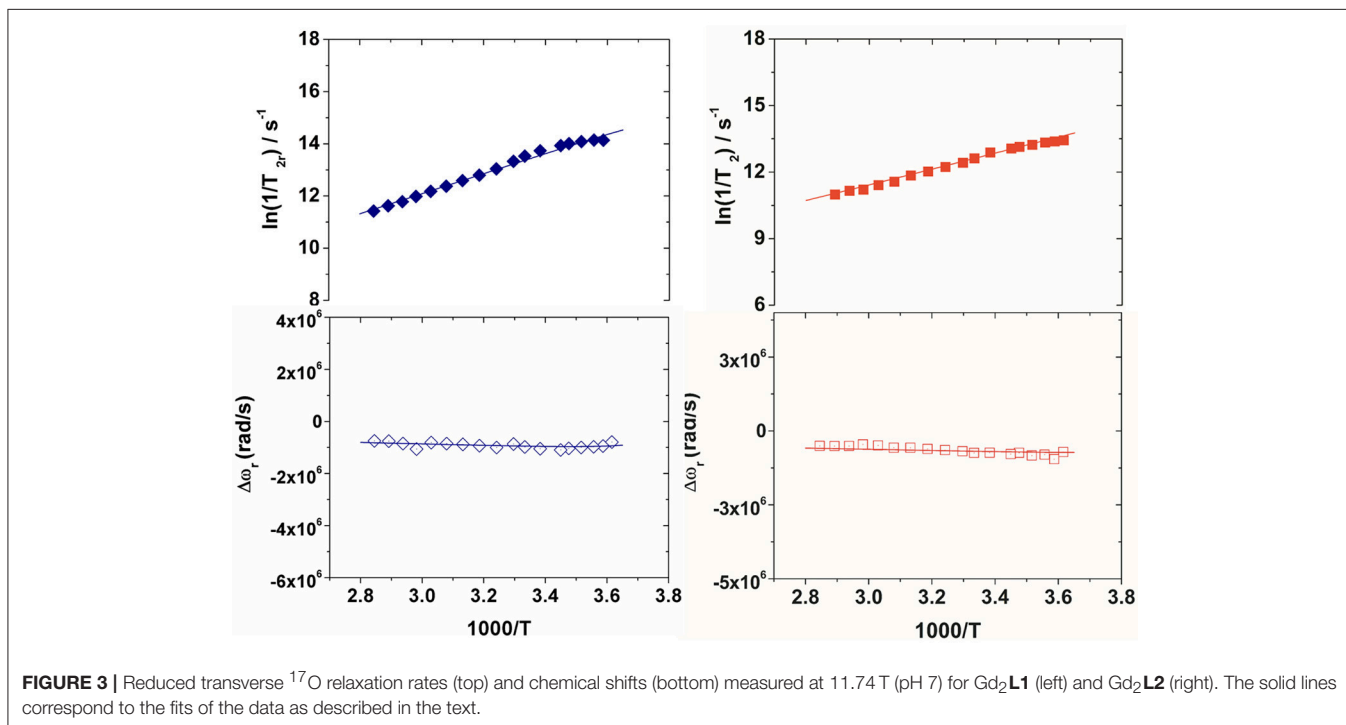
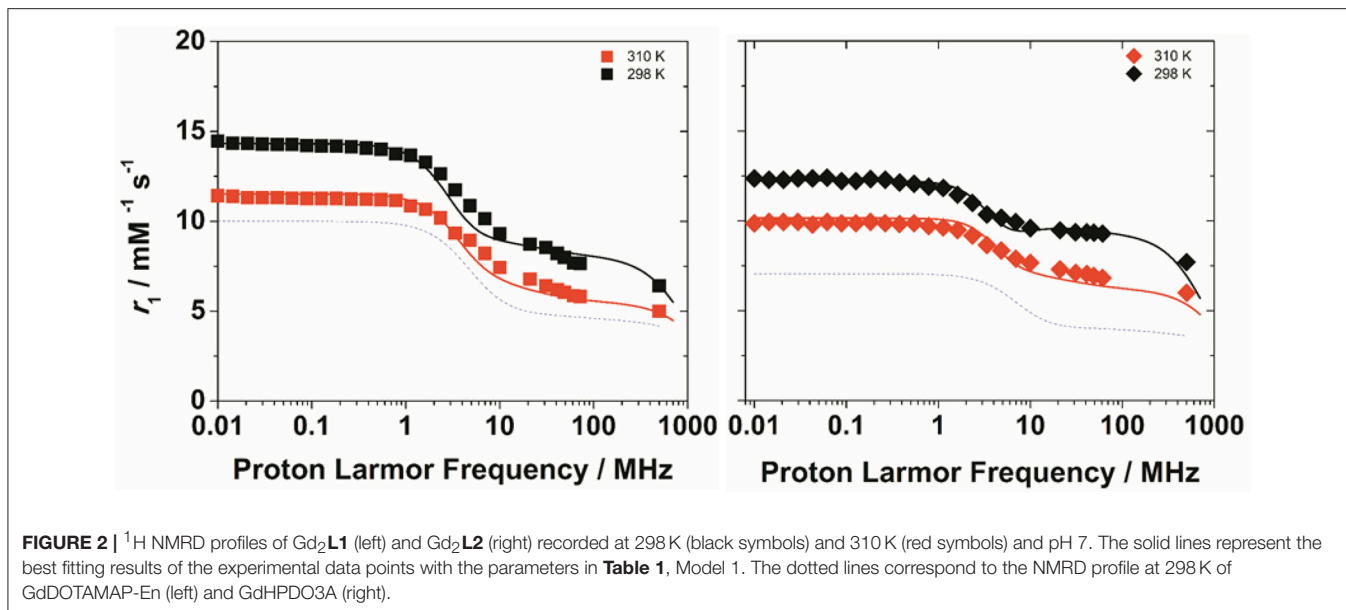
To get more insight into the physico-chemical characteristics of these novel ditopic complexes, a detailed ^1H and ^{17}O NMR relaxometric study was carried out. The magnetic field dependence of r_1 , the so-called nuclear magnetic relaxation dispersion (NMRD) profiles, were measured at 25 and 37°C in the proton Larmor frequency range 0.01–500 MHz, corresponding to magnetic field strengths varying between $2.34 \times 10^{-4} \text{ T}$ and 11.7 T (**Figure 2**). The shape of the NMRD profiles and their temperature dependence (r_1 decreases with increasing temperature, Figures S3, S4) reproduce the general behavior of small Gd^{III} complexes, characterized a plateau at low fields, a dispersion around 4–6 MHz and another region at high fields ($> 20 \text{ MHz}$) where r_1 is almost constant or changes very little. The lower values of the relaxivity at 37°C , over the entire range of proton Larmor frequencies investigated, indicate that r_1 is not limited by the water exchange rate (*fast exchange regime*) but rather by the rotational motion, as for the related monomeric complexes. A least-square fit of the profiles was carried out in terms of the established theory of paramagnetic relaxation expressed by the Solomon-Bloembergen-Morgan (Bloembergen and Morgan, 1961) and Freed's (Freed, 1978) equations for the *inner-* (IS) and *outer sphere* (OS) proton relaxation mechanisms, respectively. Because of the large number of parameters involved in the fitting procedure, some of them are usually fixed to known or reasonable values. The hydration number q was fixed to 1; the distance between Gd^{3+} and the protons of the bound water molecule, r , was fixed to 3.0 Å; the distance of closest approach, a , of the *outer sphere* water molecules to Gd^{3+} was set to 4.0 Å and for the relative diffusion coefficient D standard values of 2.24 and $3.1 \times 10^{-5} \text{ cm}^2 \text{ s}^{-1}$ (298 and 310 K) were used. The fit was performed using as adjustable parameters τ_R and the electronic relaxation parameters Δ^2 (trace of the squared zero-field splitting, ZFS, tensor) and τ_V (correlation time for the modulation of the transient ZFS).

The residence lifetime of coordinated water, τ_M , does not affect the relaxivity of the systems under the regime of fast exchange. However, the accurate value of this parameter can

be obtained through the measurement of the temperature dependence of the ^{17}O NMR transverse relaxation rate, R_2 , and paramagnetic shift, $\Delta\omega$, of the solvent water. The data were measured at 11.7 T on 20 and 16 mM solutions of $\text{Gd}_2\text{L1}$ and $\text{Gd}_2\text{L2}$, respectively, at neutral pH. The experimental data are often reported as reduced transverse relaxation rates, R_{2r} , defined as $1/T_{2r} = R_{2r} = R_{2p}/p_M$, where p_M is the molar fraction of inner-sphere water molecules. The reduced transverse ^{17}O -relaxation rates and chemical shifts ($\Delta\omega_r$) measured for GdL1 and GdL2 are reported in **Figures 3, 4**. In both cases $1/T_{2r}$ increases with decreasing temperature over the temperature range studied (275–352 K), indicating high rate of exchange for the bound water molecule. The data were analyzed in terms of the Swift-Connick theory for ^{17}O relaxation (Swift and Connick, 1962) using as fitting parameters Δ^2 , τ_V , the τ_M value at 298 K, its enthalpy of activation ΔH_M , the scalar $\text{Gd}^{3+}\text{-}^{17}\text{O}_w$ coupling constant A/h . Moreover, the temperature dependence of τ_V and τ_R has been considered through their activation energies E_V , set to 1.0 kJ mol^{-1} , and E_R , fixed to 18.0 kJ mol^{-1} . The best-fit parameters are listed in **Table 1** and compared with those previously reported for the related mononuclear complexes.

The k_{ex} value obtained for $\text{Gd}_2\text{L1}$ ($1.0 \times 10^8 \text{ s}^{-1}$; **Table 1**) is quite similar to that of the parent GdDOTAMAP-En complex, indicating that the formation of the ditopic complex did not significantly alter the coordination geometry around the metal ion. In the case of $\text{Gd}_2\text{L2}$, the residence lifetime of the bound water molecule is quite short (5.0 ns) thus suggesting that, unlike the case of the monomeric GdHPDO3A complex, the formation of the dimer involves the occurrence of a predominant population of fast-exchanging TSAP isomer.

The experimental NMRD curves were first analyzed with a model (Model 1) that takes into account the presence of only IS and OS contributions to relaxivity. The profiles are rather well reproduced with the set of parameters listed in **Table 1**, which clearly show that the r_1 values of the dimeric complexes and their frequency dependence may be attributed predominantly to the slowdown of the rotational motion and then to the longer τ_R values. For $\text{Gd}_2\text{L1}$ the increase in the τ_R value with respect to the value reported for GdDOTAMAP-En is 114%. Therefore, the binuclear complex presents a remarkable stereochemical rigidity



and the greater molecular mass, compared to the monomer, is entirely translated into a corresponding lengthening of τ_R . In the case of $\text{Gd}_2\text{L2}$ the value of τ_R is 215% longer than the value found for GdHPDO3A. Since the increase in the molecular mass is only of 114% is clear that the r_1 enhancement must be favored by an additional contribution. This might be identified in a sizeable second-sphere (SS) contribution, which corresponds to the presence of water molecules hydrating the complex at a distance from Gd^{3+} sufficiently short (ca. $< 4 \text{ \AA}$) and with a

residence time sufficiently long to be affected by the rotation (Botta, 2000). We analyzed the NMRD profiles considering also this possible contribution, expressed in terms of two additional parameters: the number q_{SS} of second sphere water molecules and their rotational correlation time, $\tau_{R(SS)}$ (Model 2 in **Table 1**). The average distance from the paramagnetic center has been arbitrarily fixed at 3.5 \AA , an intermediate value between those of water molecules in the inner (3.0 \AA) and outer (4.0 \AA) solvation shell (**Figure 4**). In the case of $\text{Gd}_2\text{L1}$ the best results are obtained

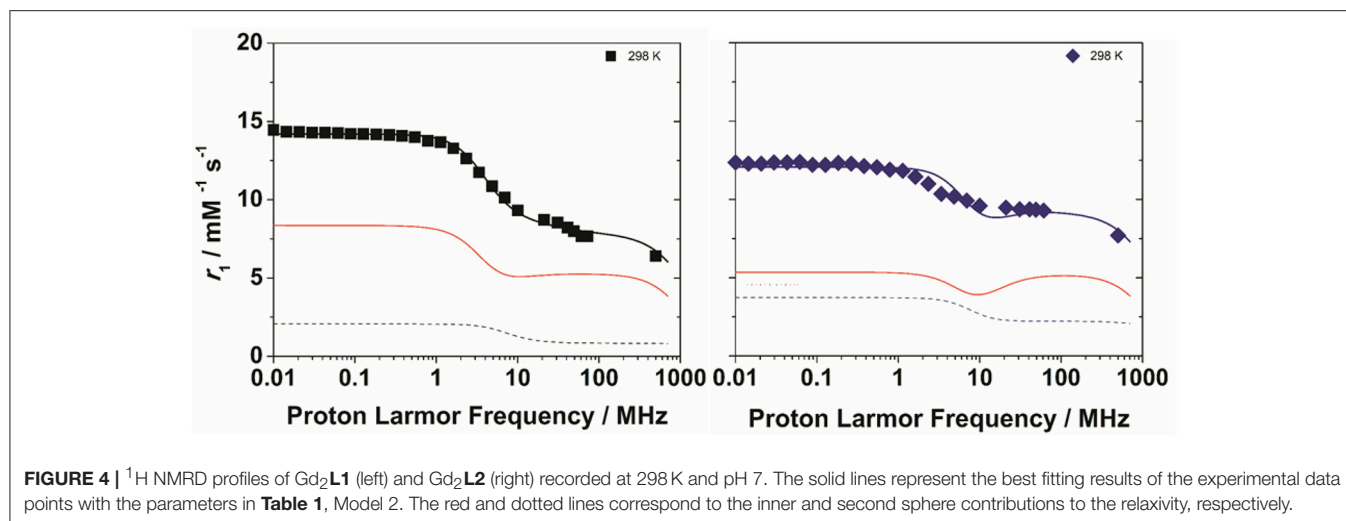


TABLE 1 | Best-fit parameters obtained from the analysis of the $1/T_1$ ^1H NMRD profiles (298 and 310 K) and ^{17}O NMR data for GdHPDO3A,^a GdDOTAMAP-En,^b Gd₂L1 and Gd₂L2^c.

Parameter	GdHPDO3A		GdDOTAMAP-En	Gd ₂ L1		Gd ₂ L2	
	SAP	TSAP		Model 1 (IS+OS)	Model 2 (IS+OS+SS)	Model 1 (IS+OS)	Model 2 (IS+OS+SS)
$^{298}r_1$ ($\text{mM}^{-1} \text{s}^{-1}$)		4.6	4.9		8.7		9.5
20 MHz							
$^{310}r_1$ ($\text{mM}^{-1} \text{s}^{-1}$)		3.6	3.9		6.8		7.3
20 MHz							
$^{298}\tau_M$ (ns)	640	8.9	12		10.0 ± 1.2		5.0 ± 0.4
$^{298}\tau_R$ (ps)		65	79	169 ± 4	140 ± 2	205 ± 3	140^c
Δ^2 (10^{19}s^{-2})	9.9	1.5	3.9	1.3 ± 0.1	1.8 ± 0.1	2.0 ± 0.1	6.2 ± 0.3
$^{298}\tau_V$ (ps)	8	30	15	40 ± 2	36 ± 2	40 ± 2	22 ± 1
ΔH_M (kJ mol^{-1})	53^d	15^d	29.7		30.6 ± 1.1		29.5 ± 1.1
A/h (10^6 rad s^{-1})		-3.5	-3.2		-3.5 ± 0.1		-3.4 ± 0.1
q_{SS}		-	-	-	2	-	4
$^{298}\tau_{R(SS)}$ (ps)		-	-	-	45 ± 2	-	60 ± 4

^a From Delli Castelli et al. (2013); ^b from Tei et al. (2009a); ^c The parameters fixed in the fitting procedure are: $q = 1$, $r_{\text{GdO}} = 2.5 \text{ \AA}$, $r_{\text{GdH}} = 3.0 \text{ \AA}$, $a_{\text{GdH}} = 4.0 \text{ \AA}$, $^{298}D_{\text{GdH}} = 2.24 \times 10^{-5} \text{ cm}^2 \text{ s}^{-1}$, $E_R = 18 \text{ kJ mol}^{-1}$, $E_V = 1 \text{ kJ mol}^{-1}$, $r_{\text{GdH(SS)}} = 3.8 \text{ \AA}$; ^d Activation energy, E.

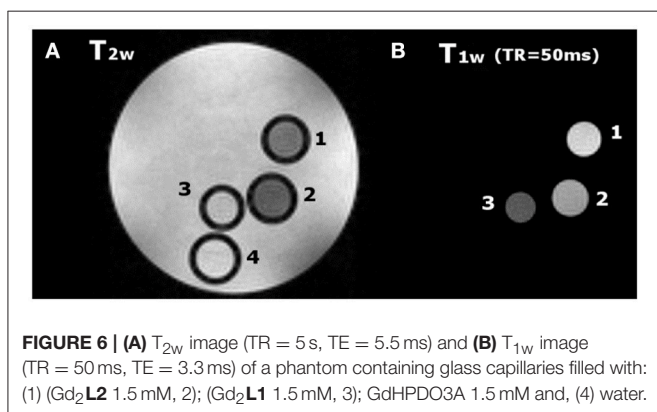
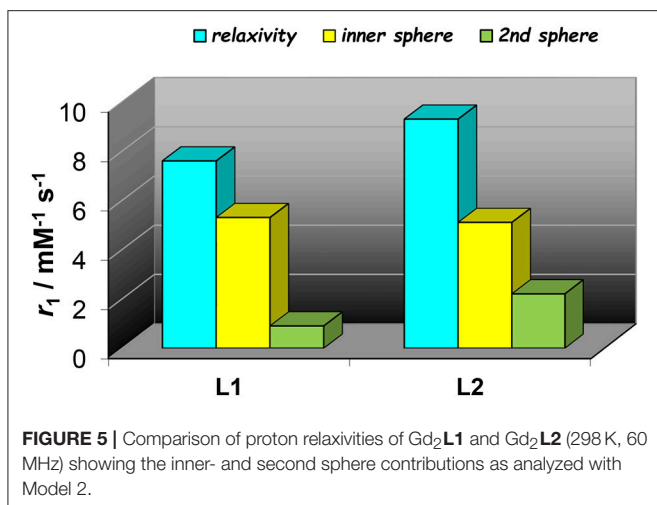
by taking into account the contribution of two water molecules belonging to the SS and characterized by a rotational correlation time $\tau_{R(SS)}$ of 45 ps. This involves consequently a decrease in the global τ_R passing from 169 to 140 ps, a value that best fits the molecular size of the complex. The same value of τ_R was used in the analysis of the NMRD profile of Gd₂L2, obtaining the best result with the additional contribution of four SS water molecules with a $\tau_{R(SS)}$ of 60 ps. As it is clearly apparent from the plot of Figure 5, the SS contribution is rather small in the case of Gd₂L1, about 12% at 1.5 T and 310 K, while it turns out to be very significant for Gd₂L2 as it can be attributed to it over 20% of the overall relaxivity measured. The greater weight of the SS contribution to Gd₂L2 is probably due to the presence of negative charges in the complex due to the deprotonation of the alcohol groups, in accordance with the CEST data.

MR Phantom Images

MR images of phantom containing glass capillaries filled with 1.5 mM water solutions of Gd₂L1, Gd₂L2, or GdHPDO3A were imaged at 7 T. T_{2w} and T_{1w} representative images are reported in Figures 6A,B, respectively. The Signal Intensity in T_{1w} image is higher in the two capillaries filled with dinuclear Gd-complexes (capillary 1 and 2 in Figure 6) with respect to that one filled with GdHPDO3A (capillary 3 in Figure 6). Furthermore, as expected, contrast enhancement provided by Gd₂L2 is visibly higher than that one provided by Gd₂L1.

Molecular Modeling on Gd₂L2

The geometry of isolated Gd₂L2 dimer was optimized at the DFT level, including a water molecule coordinated to each Gd³⁺ ion; to simulate the conditions at physiological pH, the



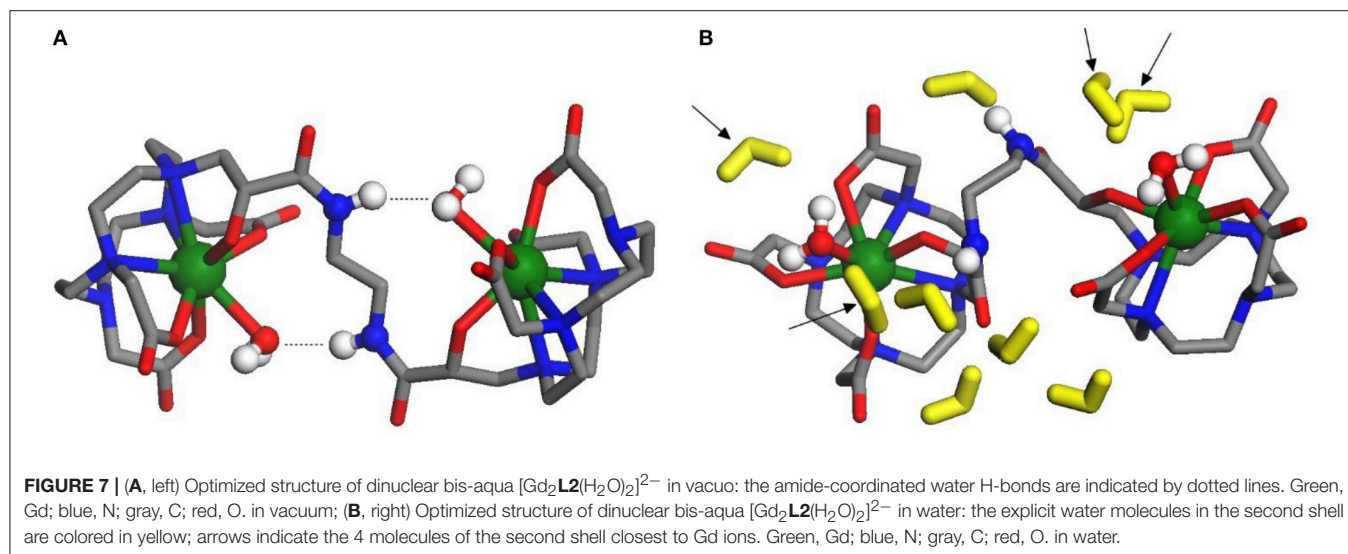
carboxylic and hydroxyl groups on both HPADO3A chelators were deprotonated, generating a double negative charge on the dimer. Then, the solvent (water) effects were included, re-optimizing the geometry with 9 water molecules in the second solvation shell and using the PCM model to account for the long range electrostatic interactions with the rest of the solvent. The optimized structures of the isolated and solvated dimer are depicted in **Figures 7A,B**, respectively. In both cases, one water molecule is coordinated to each metal ion: the complexation energies (obtained by removing one of the coordinated waters and recomputing the energy of the resulting dimer and of the water molecule alone) resulted -33.6 kJ/mol in vacuo and -22.0 kJ/mol in the solvent. Not surprisingly, solvent effects weaken the coordination bond since the separated fragments, especially the charged Gd^{III} complex, can be “surrounded” by the polarized continuum better than the initial structure, so their solvation energy is higher.

In the isolated dimer (**Figure 7A**), due to the H-bonds between amide groups and coordinated waters, the dihedral angle of the N-C-C-N branch connecting the two GdHPADO3A moieties is close to 180° , so that the Gd-H₂O bond directions are almost opposite to each other. This arrangement changes when the solvent is added, since the amide groups prefer to

bind to water molecules in the second solvation shell, which are more free to move improving the H-bond stability: as a consequence, the dihedral angle is optimized around 104° and the Gd-H₂O bonds are much more parallel than in the former case. The distance of the coordinated water hydrogen atoms from Gd is 2.8/2.9 Å both in vacuo and in solution. In the latter structure, two water molecules of the second solvation shell are quite close to each GdHPDO3A moiety (indicated by arrows in **Figure 7B**): the distance of their hydrogens from Gd is 3.2–4.8 Å, a range in fair agreement with the NMR relaxometric results above described. It is also interesting to compute the energy profile for the rotation of the GdHPDO3A ends around the N-C-C-N branch, since this parameter has been shown to be critical in assessing the relaxation efficacy. Thus, we have performed a rigid scan of the dinuclear Gd₂L2 complex with respect to this dihedral angle in vacuo (**Figures S5**) and in water (**Figure S6**): in the latter case, each second shell water molecule was attributed to the closer GdHPDO3A moiety and moved along with it during the scan. The energy curves along this rotation are quite different in vacuo and in the presence of solvent molecules. As discussed above, the isolated dimer is stabilized when the Gd-cages are oriented in opposite directions, and a barrier of around 40 kJ mol⁻¹ is required to break the intramolecular H-bonds and rotate the two units. On the other hand, more than one energy minimum is found for the solvated dimer, reflecting the larger number of intermolecular interactions available with the water molecules. The computed rotational barrier is higher, around 120 kJ mol⁻¹, although this result is likely overestimated for the presence of a limited number of solvent molecules, which do not describe the solvation shell for all the conformations with the same accuracy. In any case, we can safely conclude that a high rotational barrier is also expected in aqueous solution.

CONCLUSIONS

Dinuclear Gd^{III} and Eu^{III} complexes based on two well-established $q = 1$ monomeric chelates derived from the macrocyclic systems HPDO3A and DOTAMAP were successfully synthesized via a multi-step procedure. The macrocyclic structure of the complexes guarantees the excellent thermodynamic stability and kinetic inertness of the parent complexes. While the Ln₂L1 complexes are electrically neutral, with the propionamide moiety coordinating the Ln-center, from CEST measurements on the Eu₂L2 complex we could conclude that the hydroxyl groups of the ligand H₂L2 deprotonates around physiological pH and coordinate tightly the metal center; hence, the Ln₂L2 complexes are dianionic. This hypothesis finds further support on the ¹H and ¹⁷O relaxometric data, which showed a fast water exchange rate in Gd₂L2, much faster than that found for the neutral GdHPDO3A, and a sizeable (ca. 20%) contribution of second sphere water molecules present in the surroundings of the GdHPADO3A cage. A model in which four SS water molecules at a relatively short distance from the Gd-center and with $\tau_{R(SS)}$ of 60 ps was considered to account for the large relaxivity enhancement found for the dinuclear



Gd_2L_2 with respect to the mononuclear GdHPDO3A ($r_1 = 9.5$ vs. $4.6 \text{ mM}^{-1}\text{s}^{-1}$, at 20 MHz and 298 K). This additional contribution was necessary because the relaxivity gain exceeds the increase in the molecular correlation time associated with the corresponding increase in molecular size. In the case of Gd_2L_1 , both models of analysis provide reasonable results, thus indicating the occurrence of a much lower SS contribution. The relaxometric results also confirm a high rigidity of both dinuclear complexes with a hindered or slow rotation through the linker connecting the two cages. These conclusions are further supported by the molecular modeling at the DFT level on Gd_2L_2 , which identifies a group of water molecules in well-defined positions around the metal center and at a distance quite comparable with that estimated from relaxometric data. In addition, the calculations highlight the occurrence of a high energy barrier for the rotation through the C-C bond of the ethylene linker.

These experimental results confirm that simple systems like dinuclear Gd-complexes afford optimal results in terms of relaxivity enhancement at high field strengths, as shown by the phantom MR-images at 7 T, provided they are compact, stereochemically rigid, characterized by predominantly isotropic rotational motion. An additional relevant contribution arises from the presence of a well-defined second hydration sphere. Gd_2L_2 features all these characteristics that provide an efficacy as relaxation agent over 110% higher (per Gd) than that of the clinically used MRI probes.

REFERENCES

- Aime, S., Botta, M., Ermondi, G., Fedeli, F., and Uggeri, F. (1992). Synthesis and NMRD studies of gadolinium(3+) complexes of macrocyclic polyamino polycarboxylic ligands bearing β -benzyloxy- α -propionic residues. *Inorg. Chem.* 31, 1100–1103. doi: 10.1021/ic00032a035
- Becke, A. D. (1993). Density functional thermochemistry. III. The role of exact exchange. *J. Chem. Phys.* 98, 5648–5652. doi: 10.1063/1.464913

ETHICS STATEMENT

As the study presented in the manuscript does not involve human or animal subjects, an ethics approval was not required as per institutional and national guidelines.

AUTHOR CONTRIBUTIONS

LL: performed chemical synthesis and relaxometric measurements; GF: performed the CEST experiments and the MR phantom Images. MC: performed the DFT study; LT, MB, and MC: performed interpretation of data and critically reviewed the manuscript; LT and MB: wrote the manuscript. All authors approved the final version of the manuscript.

ACKNOWLEDGMENTS

LT and MB acknowledge the support of the Università del Piemonte Orientale for (Research grant 2016). GF acknowledges Fondazione Italiana per la Ricerca sul Cancro (FIRC) for his fellowship.

SUPPLEMENTARY MATERIAL

The Supplementary Material for this article can be found online at: <https://www.frontiersin.org/articles/10.3389/fchem.2018.00158/full#supplementary-material>

- Bloembergen, N., and Morgan, L. O. (1961). Proton relaxation times in paramagnetic solutions. Effects of electron spin relaxation. *J. Chem. Phys.* 34, 842–850. doi: 10.1063/1.1731684
- Boros, E., Polasek, M., Zhang, Z., and Caravan, P. (2012). Gd(DOTA)l: a single amino acid Gd-complex as a modular tool for high relaxivity MR contrast agent development. *J. Am. Chem. Soc.* 134, 19858–19868. doi: 10.1021/ja309187m

- Botta, M. (2000). Second coordination sphere water molecules and relaxivity of gadolinium(III). *Eur. J. Inorg. Chem.* 2000, 399–407. doi: 10.1002/(SICI)1099-0682(200003)2000:3<399::AID-EJIC399>3.0.CO;2-B
- Botta, M., and Tei, L. (2012). Relaxivity enhancement in macromolecular and nanosized Gd^{III}-Based MRI contrast agents. *Eur. J. Inorg. Chem.* 1945–1960. doi: 10.1002/ejic.201101305
- Caravan, P., Cloutier, N. J., Greenfield, M. T., McDermaid, S. A., Dunham, S. U., Bulte, J. W., et al. (2002). The interaction of MS-325 with human serum albumin and its effect on proton relaxation rates. *J. Am. Chem. Soc.* 124, 3152–3162. doi: 10.1021/ja017168k
- Caravan, P., Ellison, J. J., McMurry, T. J., and Lauffer, R. B. (1999). Gadolinium(III) Chelates as MRI contrast agents: structure, dynamics, and applications. *Chem. Rev.* 99, 2293–2352. doi: 10.1021/cr980440x
- Caravan, P., Farrar, C. T., Frullano, L., and Uppal, R. (2009). Influence of molecular parameters and increasing magnetic field strength on relaxivity of gadolinium- and manganese-based T1 contrast agents. *Contrast Media Mol. Imaging* 4, 89–100. doi: 10.1002/cmimi.267
- Cossi, M., Rega, N., Scalmani, G., and Barone, V. (2003). Energies, structures, and electronic properties of molecules in solution with the C-PCM solvation model. *J. Comp. Chem.* 24, 669–681. doi: 10.1002/jcc.10189
- Delli Castelli, D., Caligara, M. C., Botta, M., Terreno, E., and Aime, A. (2013). Combined high resolution NMR and ¹H and ¹⁷O relaxometric study sheds light on the solution structure and dynamics of the lanthanide(III) complexes of HPDO3A. *Inorg. Chem.* 52, 7130–7138. doi: 10.1021/ic400716c
- Delli Castelli, D., Ferrauto, G., Cutrin, J. C., Terreno, E., and Aime, S. (2014). *In vivo* maps of extracellular pH in murine melanoma by CEST-MRI. *Magn. Reson. Med.* 71, 326–332. doi: 10.1002/mrm.24664
- Dolg, M., Stoll, H., Savin, A., and Preuss, H. (1989). Energy-adjusted pseudopotentials for the rare earth elements. *Theor. Chim. Acta* 75, 173–194. doi: 10.1007/BF00528565
- Ferrauto, G., Aime, S., McMahan, M. T., Morrow, J. R., Snyder, E. M., Li, A., et al. (2017). “Chemical exchange saturation transfer (CEST) contrast agents,” in *Contrast Agents for MRI: Experimental Methods*, eds V. C. Pierre and M. J. Allen (Cambridge, UK: RSC Publishing), 243–317.
- Fontes, A., Karimi, S., Helm, L., Yulikov, M., Ferreira, P. M., and André J. P. (2015). Dinuclear DOTA-based Gd^{III} chelates – revisiting a straightforward strategy for relaxivity improvement. *Eur. J. Inorg. Chem.* 1579–1591. doi: 10.1002/ejic.201403159
- Freed, J. H. (1978). Dynamic effect of pair correlation functions on spin relaxation by translational diffusion in liquids. II. Finite jumps and independent τ_1 processes. *J. Chem. Phys.* 69, 4034–4037. doi: 10.1063/1.436302
- Frisch, M. J., Trucks, G. W., Schlegel, H. B., Scuseria, G. E., Robb, M. A., Cheeseman, J. R., et al. (2016). *Gaussian 16, Revision A.03 Gaussian*. Wallingford, CT: Gaussian, Inc.
- Geraldes, C. F., and Laurent, S. (2009). Classification and basic properties of contrast agents for magnetic resonance imaging. *Contrast Media Mol. Imaging* 4, 1–23. doi: 10.1002/cmimi.265
- Grimme, S., Antony, J., Ehrlich, S., and Krieg, H. (2010). A consistent and accurate Ab initio parametrization of density functional dispersion correction (DFT-D) for the 94 elements H–Pu. *J. Chem. Phys.* 132:154104. doi: 10.1063/1.3382344
- Hay, P. J., and Wadt, W. R. (1985a). Ab initio effective core potentials for molecular calculations. Potentials for the transition metal atoms Sc to Hg. *J. Chem. Phys.* 82, 270–283.
- Hay, P. J., and Wadt, W. R. (1985b). Ab initio effective core potentials for molecular calculations. Potentials for K to Au including the outermost core orbitals. *J. Chem. Phys.* 82, 299–310. doi: 10.1063/1.448975
- Helm, L. (2010). Optimization of gadolinium-based MRI contrast agents for high magnetic-field applications. *Future Med. Chem.* 2, 385–396. doi: 10.4155/fmc.09.174
- Lawson, D., Barge, A., Terreno, E., Parker, D., Aime, S., and Botta, M. (2015). Optimizing the high-field relaxivity by self-assembling of macrocyclic Gd(III) complexes. *Dalton Trans.* 44, 4910–4917. doi: 10.1039/C4DT02971B
- Merbach, A. E., Helm, L., and Tóth, É. (2013). *The Chemistry of Contrast Agents in Medical Magnetic Resonance Imaging, 2nd Edn*. New York, NY: John Wiley & Sons.
- Nicholls, F. J., Ling, W., Ferrauto, G., Aime, S., and Modo, M. (2015). Simultaneous MR imaging for tissue engineering in a rat model of stroke. *Sci. Rep.* 5:14597 doi: 10.1038/srep14597
- Powell, D. H., Dhubhghaill, O. M. N., Pubanz, D., Helm, L., Lebedev, Y. S., Schlaepfer, W., et al. (1996). Structural and dynamic parameters obtained from ¹⁷O NMR, EPR, and NMRD studies of monomeric and dimeric Gd³⁺ complexes of interest in magnetic resonance imaging: an integrated and theoretically self-consistent approach. *J. Am. Chem. Soc.* 118, 9333–9346. doi: 10.1021/ja961743g
- Pumphrey, A., Yang, Z., Ye, S., Powell, D. K., Thalman, S., Watt, D. S., et al. (2016). Advanced cardiac chemical exchange saturation transfer (cardioCEST) MRI for *in vivo* cell tracking and metabolic imaging. *NMR Biomed.* 29, 74–83. doi: 10.1002/nbm.3451
- Ranganathan, R. S., Fernandez, M. E., Kang, S. I., Nunn, A. D., and Ratsep, P. C., Pillai, K. M., et al. (1998). New multimeric magnetic resonance imaging agents. *Invest. Radiol.* 33, 779–797. doi: 10.1097/00004424-199811000-00002
- Rotz, M. W., Culver, K. S. B., Parigi, G., MacRenaris, K. W., Luchinat, C., Odom, T. W., et al. (2015). High relaxivity Gd(III)_DNA gold nanostars: investigation of shape effects on proton relaxation. *ACS Nano* 9, 3385–3396. doi: 10.1021/nn5070953
- Rudovský, J., Botta, M., Hermann, P., Koridze, A., and Aime, S. (2006). Relaxometric and solution NMR structural studies on ditopic lanthanide(III) complexes of a phosphinate analogue of DOTA with a fast rate of water exchange. *Dalton Trans.* 2323–2333. doi: 10.1039/b518147j
- Stancanello, J., Terreno, E., Delli Castelli, D., Cabella, C., Uggeri, F., and Aime, S. (2008). Development and validation of a smoothing-splines-based correction method for improving the analysis of CEST-MR images. *Contrast Media Mol. Imaging* 4, 136–149. doi: 10.1002/cmimi.240
- Swift, T. J., and Connick, R. E. J. (1962). NMR-relaxation mechanisms of O17 in aqueous solutions of paramagnetic cations and the lifetime of water molecules in the first coordination sphere. *J. Chem. Phys.* 37, 307–319. doi: 10.1063/1.1701321
- Tei, L., Baranyai, Z., Gaino, L., Forgács, A., Vágner, A., and Botta, M. (2015). Thermodynamic stability, kinetic inertness and relaxometric properties of monoamide derivatives of lanthanide(III) DOTA complexes. *Dalton Trans.* 44, 5467–5478. doi: 10.1039/C4DT03939D
- Tei, L., Gugliotta, G., Avedano, S., Giovenzana, G. B., and Botta, M. (2009a). Application of the Ugi four component reaction to the synthesis of ditopic bifunctional chelating agents. *Org. Biomol. Chem.* 7, 4406–4414. doi: 10.1039/b907932g
- Tei, L., Gugliotta, G., Baranyai, Z., and Botta, M. (2009b). A new bifunctional Gd^{III} complex of enhanced efficacy for MR-molecular imaging applications. *Dalton Trans.* 9712–9714. doi: 10.1039/b917566k
- Terreno, E., Stancanello, J., Longo, D., Delli Castelli, D., Milone, L., Sanders, H. M., et al. (2009). Methods for an improved detection of the MRI-CEST effect. *Contrast Media Mol. Imaging* 5, 237–247. doi: 10.1002/cmimi.290
- Tircsó, G., Kovacs, Z., and Sherry, A. D. (2006). Equilibrium and formation/dissociation kinetics of some Ln(III)/PCTA complexes. *Inorg. Chem.* 45, 9269–9280. doi: 10.1021/ic0608750
- Vagner, A., Gianolio, E., Aime, A., Maiocchi, A., Toth, I., Baranyai, Z., et al. (2016). High kinetic 38 inertness of a bis-hydrated Gd-complex with a constrained AAZTA-like ligand. *Chem. Commun.* 52, 11235–11239. doi: 10.1039/C6CC04753J
- Wadt, W. R., and Hay, P. J. (1985). Ab initio effective core potentials for molecular calculations. Potentials for main group elements Na to Bi. *J. Chem. Phys.* 82, 284–298.

Conflict of Interest Statement: The authors declare that the research was conducted in the absence of any commercial or financial relationships that could be construed as a potential conflict of interest.

The reviewer, EC, and handling Editor declared their shared affiliation.

Copyright © 2018 Leone, Ferrauto, Cossi, Botta and Tei. This is an open-access article distributed under the terms of the Creative Commons Attribution License (CC BY). The use, distribution or reproduction in other forums is permitted, provided the original author(s) and the copyright owner are credited and that the original publication in this journal is cited, in accordance with accepted academic practice. No use, distribution or reproduction is permitted which does not comply with these terms.